



Preliminary test and analysis of an ultralight lenticular tube based on shape memory polymer composites

Zhengxian Liu^a, Qifeng Li^a, Wenfeng Bian^b, Xin Lan^c, Yanju Liu^a, Jinsong Leng^{c,*}

^a Department of Astronautical Science and Mechanics, Harbin Institute of Technology (HIT), Harbin 150001, People's Republic of China

^b Department of Civil Engineering, Harbin Institute of Technology (HIT), Weihai 264209, People's Republic of China

^c National Key Laboratory of Science and Technology on Advanced Composites in Special Environments, Harbin Institute of Technology (HIT), Harbin 150080, People's Republic of China

ARTICLE INFO

Keywords:

Shape memory polymer composites
Lenticular tube
Deployable space structures

ABSTRACT

Shape memory polymer composites (SMPCs) demonstrate the advantages of light weight, high strain rate, high strength, high stiffness, self-locking and self-deployment. In this study, the mechanical properties and deformation performance of SMPC-based lenticular tube are studied. Dynamic mechanical analysis (DMA) tests and three-point bending tests were carried out to determine thermomechanical properties, and $+45^\circ/-45^\circ$ fiber layout was chosen as the optimum layout. Tensile tests were conducted to investigate the mechanical properties of SMPC at different temperature. The strain distribution during recovery process was obtained by digital image correlation (DIC) experiment. Bending and recovery process were simulated by finite element analysis, the stress distribution of curved state of lenticular tube were obtained. Comparing with traditional lenticular tube, SMPC-based lenticular tube exhibits the advantages of controllability and stability in deploying process, and they still work well after folding 30 deformation cycles. Due to its above advantages, several potential applications are proposed for deployable space structures and will be validated in near future.

1. Introduction

Shape memory polymer (SMPs) [1–3] are novel and deformable polymers that can alternate between the original shape and a freely designed temporary shape. The deformation and recovery process are conceptually shown below in Fig. 1. When the temperature exceeds the glass transition temperature (T_g), it is in a rubbery state, and external force is applied to change its shape. When cooling below the T_g , the polymer chains will be frozen [4–6]; thus, the shape can be fixed. If the temperature is elevated above the T_g again, then the polymer chains will be “released” and then recovered to its original shape [3,7–9]. This phenomenon is referred to as shape memory effect. SMPs have been used broadly in smart materials and structure because of its advantages such as large deformation, low density, variable stiffness, various stimulation modes, and good biocompatibility [10–12].

Whereas SMPs do have some weakness such as low stiffness, strength, and actuation force. Therefore, they are not suitable as load-bearing structural materials. However, the occurrence of composites make up the shortcomings by adding stiff and strong reinforcements into materials, which make it possible for smart functional materials (such as SMPs) to be used in load-bearing material. And composite

materials have been widely used in aerospace because of their high strength, stiffness, stability, and ultra-low thermal expansion coefficient [11,14].

Lan [15] developed carbon fiber reinforced polymer (CFRP) hinges that can be used for deployable structures, and found that the fiber microbuckling is the main mechanism for SMPC to achieves large strain during bending. The bending angles are almost all more than 90° , but the bending strain is usually less than 5%.

Diana [16] proposed a kind of bi-stable composite cylindrical shell, and an analytical model is proposed in this article to anticipate the longitudinal and transverse curvature factors. The bending stress and geometric parameters have also been investigated in detail.

In 2017, National Aeronautics and Space Administration (NASA) [17] successfully demonstrated the newly launched solar array in space, which is more flexible, lighter and has a larger gathering and unfolding ratio than the traditional folded solar array, as is shown in Fig. 2. The solar array utilized the storage and release of material strain energy of the elastic slit tube booms to complete the structure gathering and unfolding. The tube could also be employed as the main supporting structure of deployable parabolic antennae and space solar array supporting cable networks as well [18].

* Corresponding author.

E-mail address: lengjs@hit.edu.cn (J. Leng).

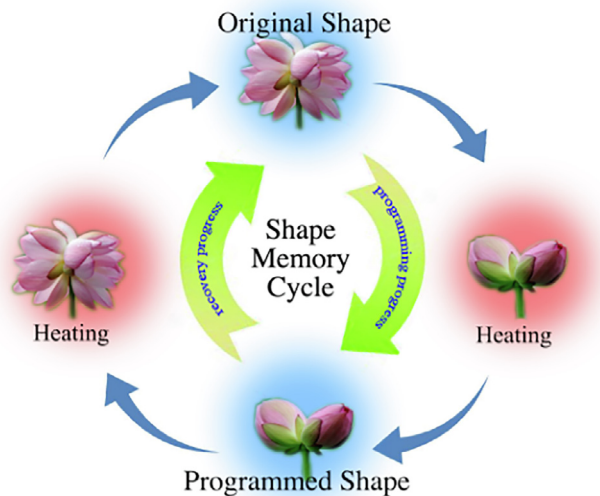


Fig. 1. The shape memory flower, representing shape memory polymers, can be deformed and recover under heating [13].

Bai [19,20] established an analytical model for ultra-thin-walled lenticular collapsible composite tube (LCCT), which can predict the in-plane strain of the LCCT during flattening and crimping. The analytical solution of inter-laminar shear stress of the LCCT was derived using the micro-balance equation. The LCCT was fabricated by vacuum-assisted resin transfer molding. Afterwards, the flattening and crimping tests were performed, while buckling deformation mechanism of the LCCT was also studied. Hu [21] studied the large deformation behaviors of the LCCT during the flattening process, and analytical models were proposed to predict the tensile and compression experiments.

The traditional ultra-thin-walled LCCT structure is deployed by the release of strain energy, which demonstrate the disadvantages of thickness limitation (Generally no more than 0.5 mm), large impact to the structure itself, too fast deployment speed, and being unable to achieve self-locking after bending [22,23]. Combining SMPC with LCCT, this paper proposes a LCCT structure based on SMPC, which are able to control the deploying process by thermal stimulation. The LCCT structure based on SMPC breaks through the limitation of traditional LCCT structure due to the shape memory effect and variable stiffness characteristics, which also makes the LCCT structure more stable and functional.

In this study, a SMPC-based LCCT structure was studied, which can realize self-locking and self-deployment. LCCT was fabricated by VARTM and resin bonding process based on the design. For the purpose of our analysis and design, the thermo-mechanical properties of the material was characterized systematically, and we focus on the thermal drive and recovery performance of SMPC-based LCCT.

2. Structure design and fabrication

2.1. Structure design

LCCT is short for lenticular collapsible composite tube [19], which describes the geometry and the feature of the tube. LCCT is mostly used in aerospace application because it can be rolled in a tiny package, and it is able to extend itself into the original shape by releasing the elastic strain energy. But this shape recovery process is not controllable, and only exhibits two states (original and final). However, with the shape memory polymer resins, the recovery process can be controlled easily and the shape can be fixed at any time during the shape recovery process (shown in Fig. 3A). The transverse section of the LCCT used in our tests is shown in Fig. 3B, in which the transverse section of the

specimens can be simplified to lenticular shells with bonded edges. The two arcs have the same radius of 17 mm, with 10 mm bonded edge on the both sides. The thickness of the LCCT is 0.8 mm. The angles between the two center of the arcs are 60° respectively (between line AB and AO in Fig. 3B).

2.2. Fabrication process

The shape memory epoxy resin adopted in this study was developed by Jinsong Leng's research group [24]. The reinforcement is the carbon fiber twill fabric (Toray, T300-3k). The shape memory composites were fabricated by vacuum-assisted resin transfer molding (VARTM) [25], in the illustration of the schematic diagram can be seen in Fig. 4.

The VARTM fabricating process is shown in Fig. 5, which follows the below sequence: a) Prepare a "Ω"-shaped mold and clean the surface with alcohol. b) Cut out an appropriately-sized carbon fiber twill fabric for use on the mold and put diversion network, porous release film, and a sealing film on the fabric. c) Adjust the vacuum pressure of the vacuum pump, and vacuum the resin. d) Put the vacuumed mold into an autoclave for curing. The temperature is set at 80 °C and 100 °C for 3 h each, 150 °C for 5 h, and the transition time of temperature is 30 min. e) Place the two lenticular shells with the same epoxy resin back into the autoclave, and fix the upper and lower molds using a clamp device; the post-curing procedure is the same as step d. f) Remove and cut out the cured lenticular tube according to the design.

3. Experiments

3.1. Dynamic mechanical analysis

In this study, DMA [26,27] (Dynamic Mechanical Analysis) of epoxy resin was conducted with a dynamic mechanical analyzer. T_g refers to the temperature where a polymer changes from glassy state to rubbery state. In other words, it represents the temperature at which an amorphous polymer (including the amorphous part of a crystalline polymer) reversibly changes from glassy state to rubbery state. The polymer shows elasticity, viscous flow and low modulus when the material is in rubbery state beyond this temperature. In this work, the thermo-dynamic properties of the composites were measured by three-point bending mode, where the effective span was set as 40 mm, and the test specimen dimensions were 60 mm (length) × 3 mm (width) × 0.5 mm (thickness). The temperature was set to increase from 0 °C to 200 °C with the growth rate of 2 °C per minute, and the loading frequency was 1 Hz.

3.2. Tensile test

The materials examined in this study were thermo-responsive SMPC, which are sensitive to temperature. In special, its mechanical properties change greatly with varying temperature, which necessitates the investigation of mechanical properties such as strength and modulus at these distinct temperatures. The materials were made by VARTM process, with one ply T300 twill fabric, the testing dimension of the samples were 150 mm (length) × 25 mm (width) × 0.54 mm (thickness). The test was conducted under the ASTM-D3039 standard with the Zwick tensile testing machine.

3.3. Bending property test

The main deformation of SMPC-based LCCT in use is the bending deformation. So that it is necessary to figure out the proper layout for laminates under bending condition. The bending properties were characterized by three-point bending tests, at the same time, it also provides great value for the design of LCCT. In this study, three kinds of shape memory composites with different laying angles (30°/60°, +45°/-45°, 0°/90°) were tested. The test process was carried out

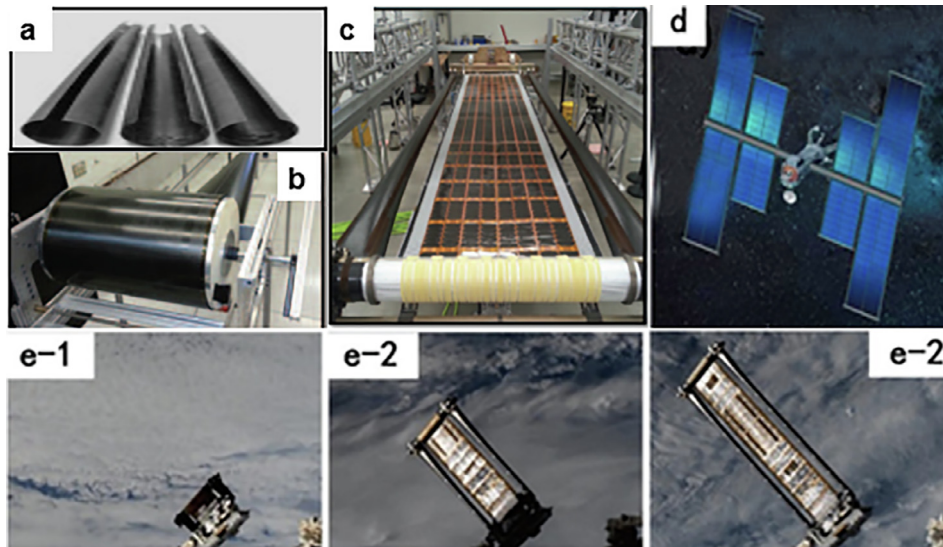


Fig. 2. Deployable solar array and its orbit verification: a) ROSA elastic slit tube booms; b) rolling state of elastic slit tube booms; c) ground deployment of the ROSA flight; d) conceptual SSL spacecraft; e) the in-orbit verification process on the international space station [17].

according to the ASTM-D790 experimental standard. The test specimen dimensions were 50.8 mm (length) × 12.70 mm (width) × 2 mm (thickness), and the effective span length was 25.4 mm.

3.4. Digital image correlation test

To study the strain distribution of the LCCT during the recovery process, the strain of single SMPC-based LCCT was examined by three-dimensional full-field strain measurement and analysis system, which is shown in Fig. 7a. The curled SMPC-based LCCT is shown in Fig. 6a, and the coating process for DIC tests are illustrated in Fig. 6b and c respectively, the surface is coated with pure white spray base then painted with random black speckles. The digital correlation method [28] is used to calculate the two images of before and after the deformation and then to acquire the displacement and deformation of the LCCT's surface. The calculation area of the test specimens is shown in Fig. 7b.

3.5. Recovery test

3.5.1. Thermal drive test

The LCCT structure based on SMPC are actuated by heating, so the easiest way of transferring heat is to bury the heating film into the material during the composites manufacturing process. However, heating film cannot endure large deformation with composite materials together, because it will lead to substantial material damage to heating

film. Therefore, the heating film is attached to the surface of the lamellar shell with a very thin tape and heated to the T_g , where the heating film resistance is 250 Ω and the size of the film is 90 mm × 240 mm.

In addition, we know that for traditional motorized LCCT structure, it can achieve different deployment rates by changing the motor speeds. Whereas SMPC-based LCCT is dominated by temperature, which is totally different from traditional LCCT structure. Since SMPCs are sensitive to the temperature, the temperature variation at different heating powers are monitored by a thermal test system (shown in Fig. 8), by which the temperature distribution on the surface of the LCCT can be visualized.

3.5.2. Recovery rate test

The recovery deformation rate of the LCCT structure was also tested in order to understand recovery process. The recovery precision of the LCCT was measured by attaching the strain gauge on the surface, and the recovery angle was recorded with measuring paper.

The test principle of shape recovery rate is shown in Fig. 9a. The strain at key point A is measured, and the strain under bending and recovery were also recorded respectively. Fig. 9b shows the four feature points on the LCCT that are tested for recovery rate. These four features are distributed at 1/4, 1/2, 3/4, and end positions of the LCCT. The strain under its initial state is ϵ_0 , when the material is in the bending storage state the strain is referred to as ϵ_s , while ϵ_r represents the strain after recovery. As such, the recovery precision can be represented as:

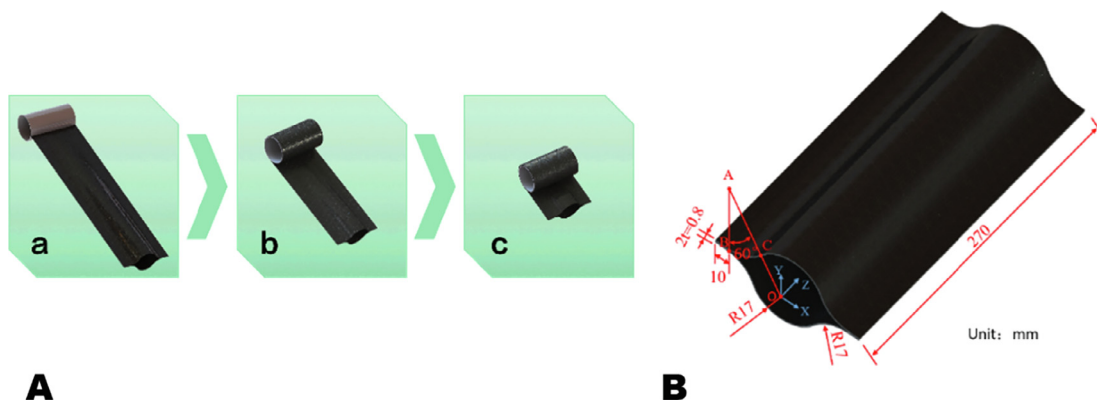


Fig. 3. Model and dimension of the LCCT: A) LCCT model; B) dimension of the transverse section area of the LCCT.

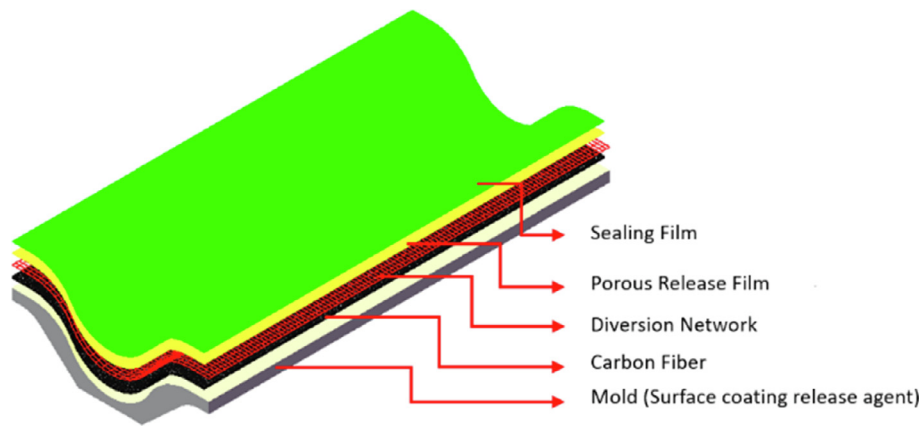


Fig. 4. Schematic diagram of VARTM.

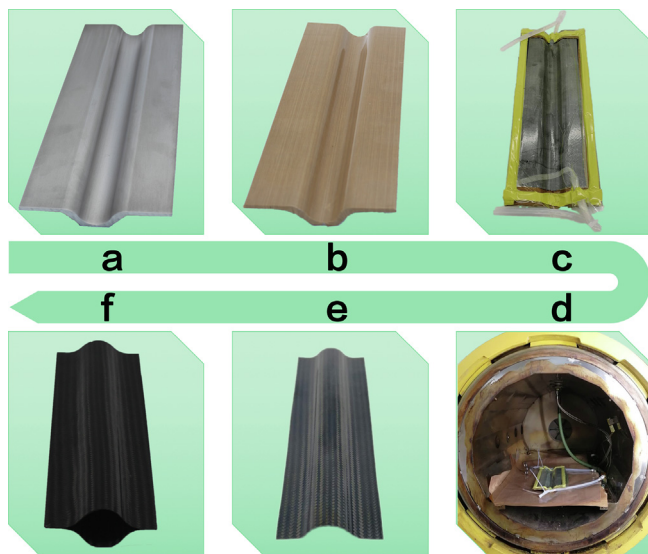


Fig. 5. Manufacturing process of the LCCT.

$$R_\epsilon = \frac{\epsilon_s - \epsilon_r}{\epsilon_s - \epsilon_o} \times 100\%$$

4. Results and discussion

4.1. Dynamic mechanical properties

In this test, two important values are taken into consideration: storage modulus and loss factor (tan δ). As shown in Fig. 10, the black line represents the storage modulus, the blue line represents loss factor, and the temperature corresponding to the peak of the loss factor is the T_g . Thus, it is found that the T_g is about 150 °C. In addition, when the

temperature is less than 150 °C, the storage modulus of the material decreases as the temperature increases. When the temperature is 150 °C, the storage modulus of the material decreases to 1.7% of room temperature, which embodies the variable stiffness characteristics of the material, and the material can be more conveniently to be shaped because of this property.

4.2. Tensile properties

The stress-strain curves of the material at different temperatures are shown in Fig. 11a. The modulus and strength of the material decrease incrementally with growing temperatures, which are shown in Fig. 11b. At 30 °C, the modulus is 22 times higher than the modulus at 150 °C, and its strength is 16 times higher than that of 150 °C. On the contrary, the elongation increases, reaching 22% when the temperature is around 120 °C, and when the temperature is near T_g , the elongation decreases to only around 4%.

Fig. 11a also illustrates that SMPC material is a material of variable stiffness that is affected by temperature. Each curve for the 30 °C, 60 °C, 90 °C and 120 °C temperature can be divided into three sections. In the 0-A section, the material is in the linear elastic stage. From the microscopic point of view, the bonding length and the bonding angle of the polymer changed because the material is being stretched, but the bonding angle is not destroyed. The A-B segment is a strain softening stage, when the stress and strain no longer maintain a linear relationship. From microscopic perspective, the polymer molecular chains are gradually destroyed with macroscopic strain softening. The B-C portion is a strain hardening stage, in which each continuous strain increase requires greater stress. Microscopically, this is due to the fact that after the molecular chains in the polymer are completely destroyed, the fiber continues to bear the load, and the macroscopic performance is strain hardening. As the temperature increases, the curve gradually becomes linear elastic. When the temperature reaches 150 °C, the polymer is in rubbery state [29], and the molecular chains are completely thawed, so elastic deformation occurs without further strain softening and

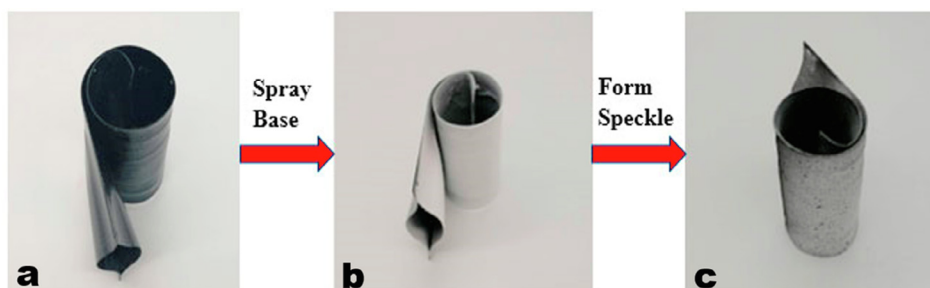


Fig. 6. Manufacturing process of DIC specimen.

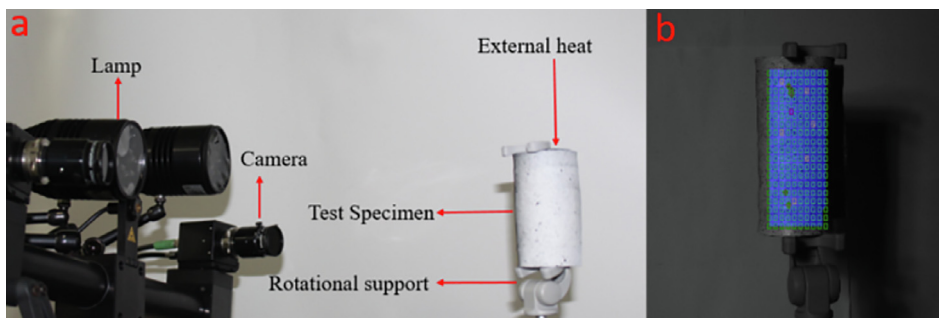


Fig. 7. DIC test diagram: a) testing process; b) calculation area.

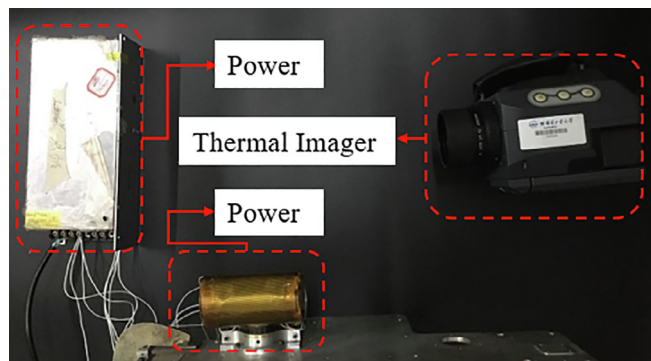


Fig. 8. Thermal test system.

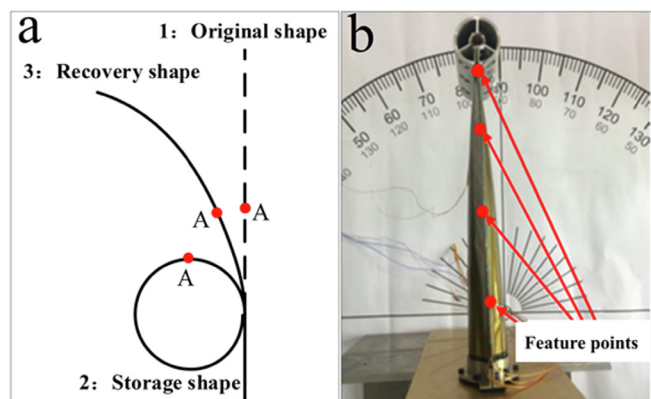


Fig. 9. Shape recovery rate: a) test principle diagram; b) feature points distribution.

hardening.

The fracture morphology of tensile tests at different temperatures is shown in Fig. 12. The fracture type differs from temperature to temperature, and it can be concluded that there are mainly two types of fracture, fiber breakage and fiber pull-out. When the temperature is at 30°, the fracture of the material occurs along fiber directions of a single 45° angle, and there is mainly fiber breakage failure, but when the temperature is at 120 °C and 150 °C, the dominant failure is fiber pull-out, and as for temperature at 60 °C and 90 °C, it is mixed failure behaviour of fiber pull-out and fiber breakage. It is reasonable because under the lower temperature, and the matrix material is in glassy state, where the toughness is relatively low, thus the fiber will began to debond from matrix, forming small cracks and eventually failed at the moment of fiber breakage. When it comes to the high temperature, the matrix material has transformed from glassy state to rubbery state, which means the toughness of matrix has improved a lot, so that fibers will easily pullout before the fiber breakage, which is also the reason for the lower strength and modulus of the material at high temperature.

4.3. Bending properties

The three-point bending displacement and load curves of the 0°/90°, 30°/60°, and +45°/−45° fiber laying angles are shown in Fig. 13. It can be seen from the diagram that the bending modulus and strength of 0°/90° laminate are the highest, but the elongation are the lowest. Conversely, the bending modulus of +45°/−45° laminate are the lowest. Whereas the elongation are the highest. For shape memory polymer composites, the bending modulus of 0°/90° laminate is 2.06 times higher than that of the 30°/60° laminate, and 3.2 times higher than that of +45°/−45° laminate. The strength of 0°/90° laminate is 1.01 times higher than that of 30°/60° layout, and 1.2 times than that of +45°/−45° respectively.

From the materials mechanics, we can get the following equation:

$$\frac{\sigma}{E} = \frac{y}{\rho I}$$

The $\frac{\sigma_s}{E}$ value is the ratio of the strength to the modulus, from which the value corresponds to the minimum value of the bending radius of the laminate of the same size and different fiber layup angle without damage, and the value also represents the toughness of the material during bending. Table 1 shows the bending modulus and strength of different fiber laying angles SMPCs. The damage of composite materials with +45°/−45° is the minimal, and when comparing with the other layering angles, the elongation for +45°/−45° is higher. Therefore, the +45°/−45° layout is employed for this study.

4.4. Digital image correlation analysis

From the DIC experiment, we can get the strain distribution of the calculation area as shown in the following Fig. 14. When the external temperature is not applied, the material is still and the strain value remains almost 0. With the stimulation of external temperature, the LCCT begins to recover. Because of the geometric symmetry of the arc section, the deformation is also symmetrical in the process of heating deformation, which is shown in Fig. 14. Although the peak value of the LCCT changes from flattening to bulging, its strain remains at a very low level, indicating that the main deformation is transferred to the arc position, and the maximum strain is 2.15%. The tensile and bending tests show that the ultimate strain of the material is 4% at about 150 °C, showing that the material will not be damaged in the process of bending and recovery.

There are some missing values when identifying the contour of the strain, this is because of the limitation of the equipment and the complexity of this type of deformation. In order to describe the strain distribution of the material section more accurately, Six feature points are respectively selected on the transverse section and the longitudinal section of the LCCT surface as shown in Fig. 15, and the strain distribution of the transverse section and the longitudinal section are as shown in Fig. 16. It can be seen that the strain variation of the surface during recovery has better symmetry along the longitudinal section, and the strain values at (C, D) are much larger than the other points on

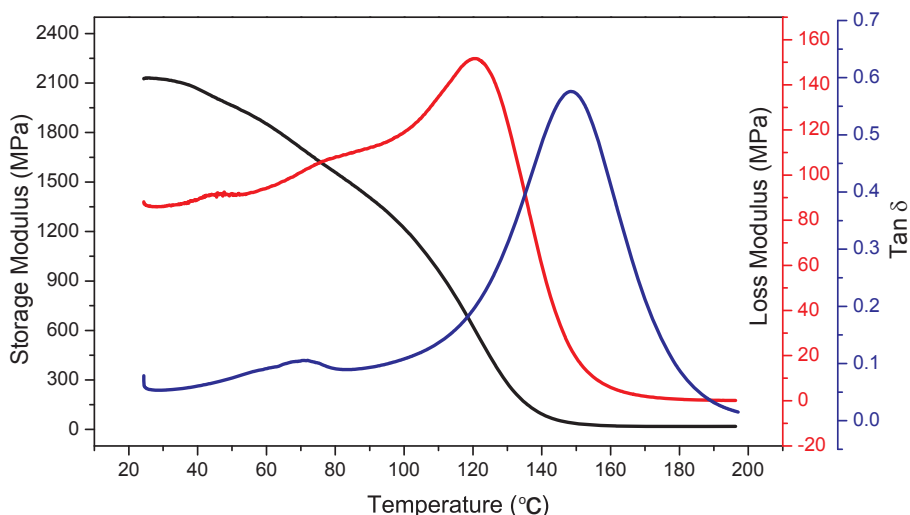


Fig. 10. DMA test results of SMP.

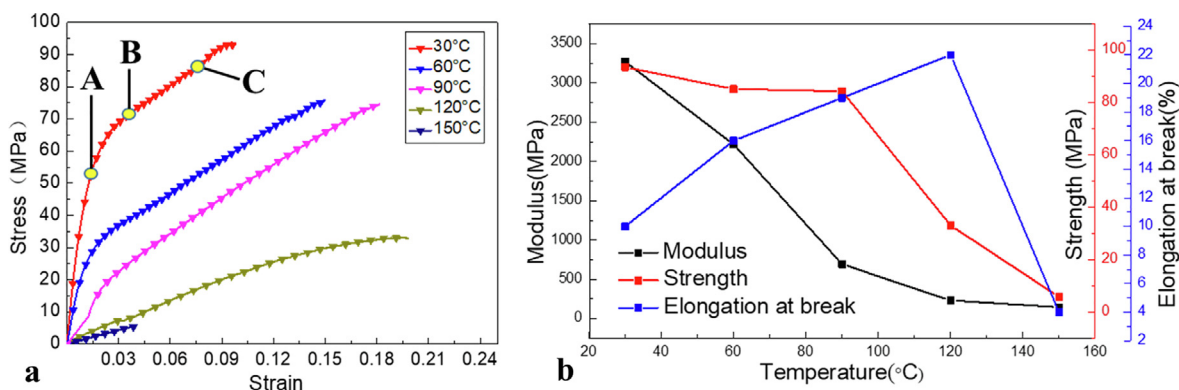


Fig. 11. Tensile test results: a) strain and stress curve; b) elongation at break, strength and modulus variation plotted against increasing temperature.

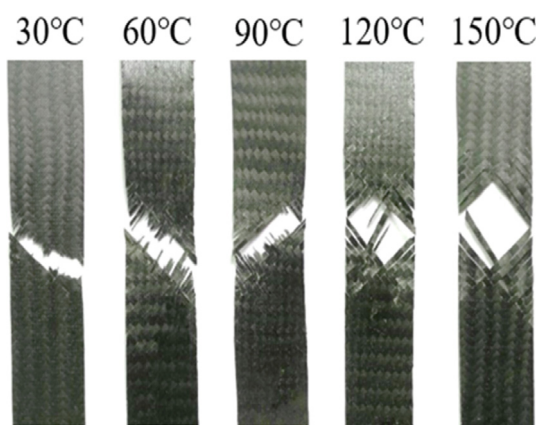


Fig. 12. Fracture shape of SMPC after the tensile test.

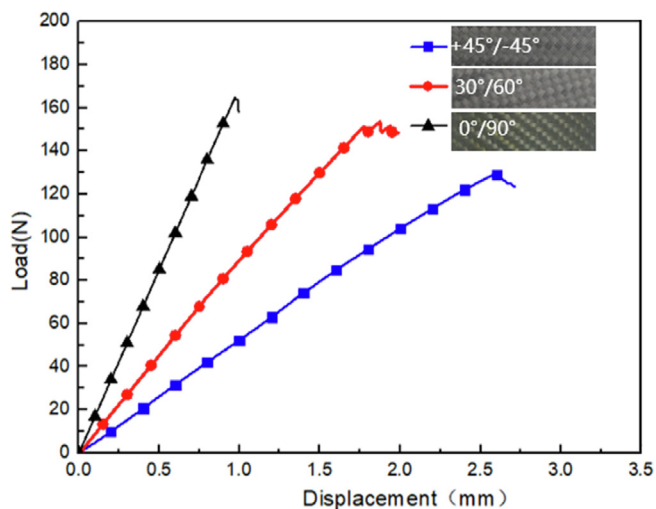


Fig. 13. Displacement and load curves of different fiber laying angles SMPCs.

the transverse section. Before the 100 s, the surface temperature of the LCCT is below 100 °C (refers to the heat distribution of the deployment process of Fig. 18), and the surface strain of the material changed is lower. The strain suddenly increases after 100 s. This is because the recovery speed of the material increases as the temperature gradually approaches the T_g . For the transverse direction, the strain increases gradually, because the selected points are in the same line, so the strain is basically the same. The strain rate increases near the T_g , and the final strain reaches about 1.2%.

Table 1
Modulus and strength of different fiber laying angles SMPCs.

Layout	30°/60°	+45°/-45°	0°/90°
Bending strength	238 MPa	203 MPa	242 MPa
Bending modulus	13.99 GPa	8.98 GPa	28.88 GPa
Strength/Modulus	1.45%	2.65%	0.84%

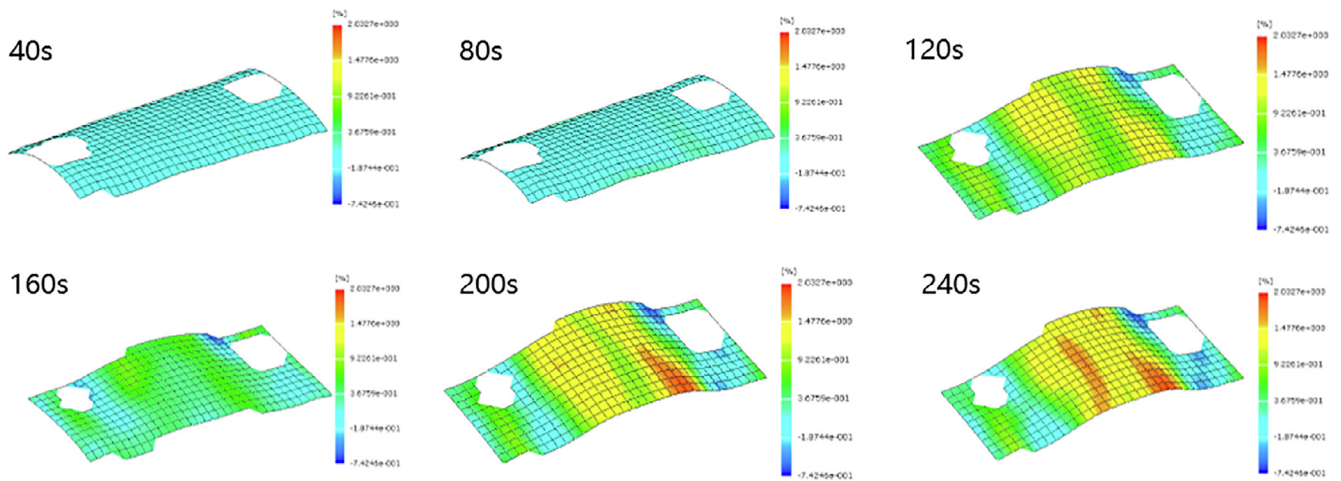


Fig. 14. Strain distribution of the LCCT during recovery process.

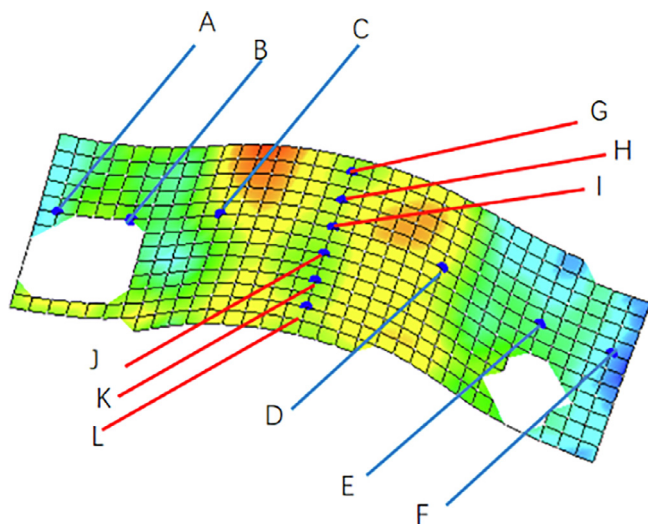


Fig. 15. Characteristic points of the LCCT surface.

4.5. Recovery properties

4.5.1. Thermal drive properties

The material's surface temperature differs under distinct heating power, and the variation is illustrated in Fig. 17. For SMPC materials, the heating curve reveals that different heating powers correspond to

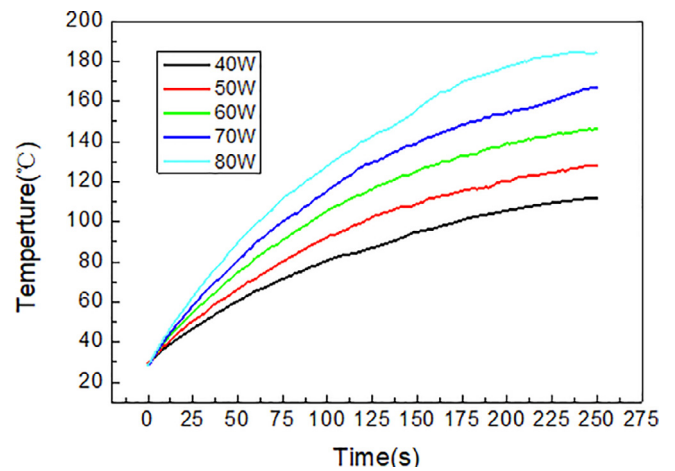


Fig. 17. Heating curve under different power.

different heating rates and equilibrium stabilization temperatures, which are the similar mechanism as the motor. It can be seen from the Fig. 17 that when the time is over 250 s, the temperature on the heating film gradually reaches the thermal equilibrium with the ambient temperature, and the temperature begins to stabilize. When the heating power is 70 W, the temperature is around 160 °C, which is slightly larger than the glass transition of the materials. Therefore, 70 W is selected as the heating power.

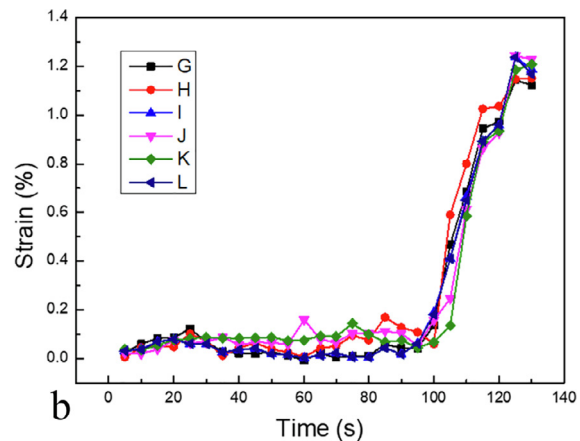
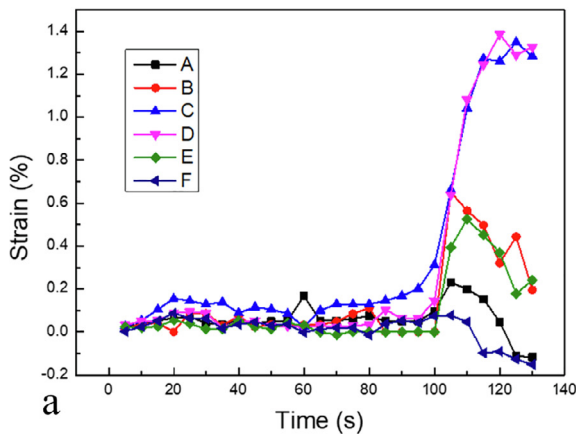


Fig. 16. Strain variation over time: a) transverse section; b) longitudinal section.

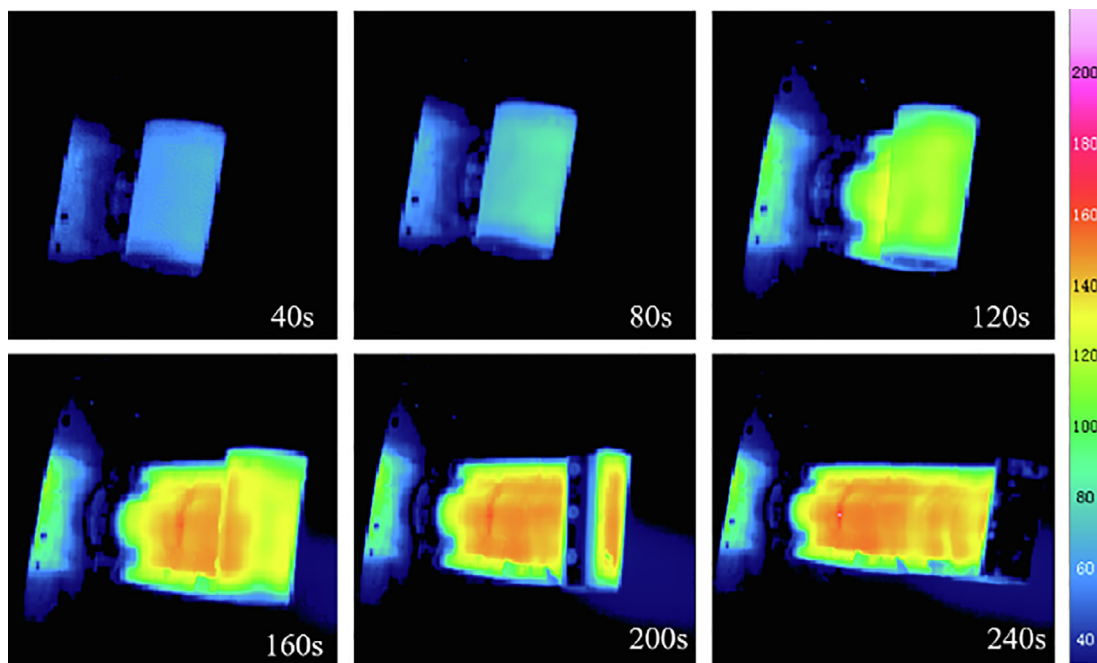


Fig. 18. Temperature distribution of the LCCT during the recovery process.

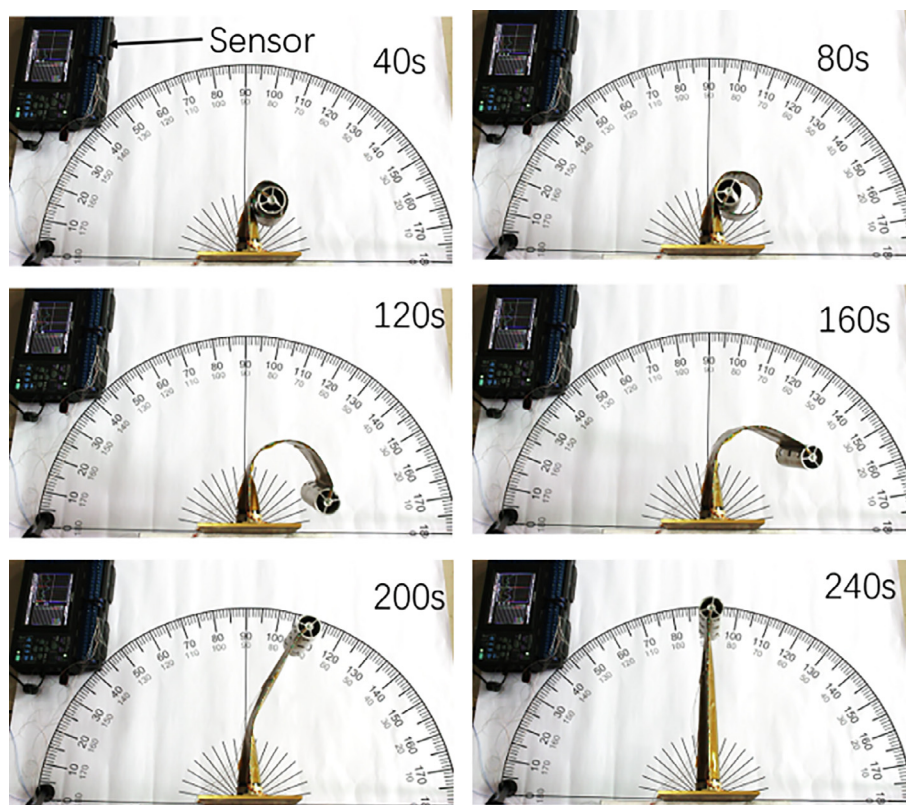


Fig. 19. Diagram of the recovery process.

The heating results are presented in Fig. 18, which shows the recovery process of the LCCT and the distribution and evolution of surface temperature. The surface temperature of the LCCT is lower than the T_g within 0–120 s, and the recovery angle is smaller. After 150 s, the recovery speed accelerates. The temperature of electric heating film reaches 150 °C after heating for approximately 150 s. At around 200 s, the surface temperature of the heating film gradually reaches equilibrium with the outside environment, and the highest temperature is

around 160 °C. From the heat distribution of the heating film on the surface of the LCCT, the temperature in the middle area is much higher, but the temperature at the edge is lower. This is because there is more heat exchange between the surrounding area and the outside, and the LCCT can recover its original shape in about 240 s.

4.5.2. Recovery rate test

The recovery process of the LCCT is shown in Fig. 19. It can be seen

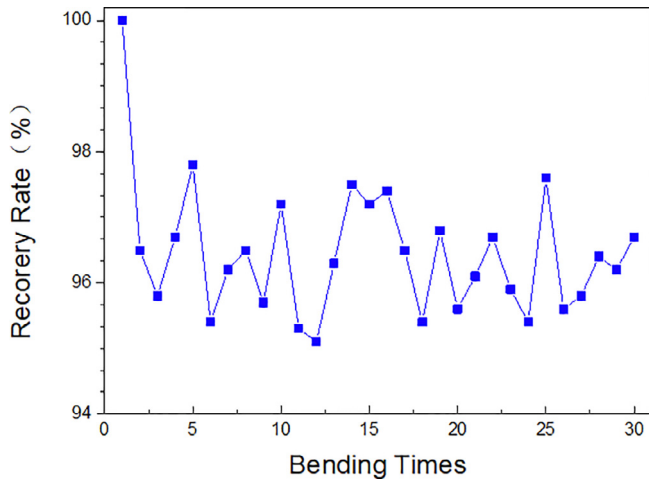


Fig. 20. Recovery rate at the end of the LCCT during 30 bending times.

that the quickest recovery occurs at 1/4 point, followed by the end position. Finally, the first three feature points recover to the vertical state with a recovery rate of 100%. The recovery rate of the end of the LCCT is 99%. The reason for the failure to recovery 100% is likely that the end position is assembled with a metal load of 0.2 kg, which takes most of the heat away, leading to a temperature drop in the end part, the other possible reason is the damage to the sheet during large bending deformation.

It can be seen from the graph that the recovery rate of all parts except the load end can reach 100%. The low recovery rate of the load end is due to the irreversible damage caused by the small radius of rotation of the root during the initial bending. The bending damage of the material will be discussed in more detail in future research. Fig. 20 shows the shape recovery rate at the end part of the tube after 30 deformation cycles. It is shown that the average shape recovery rate at the end of tube can reach more than 96.2%, even after 30 deformation cycles.

5. Simulation for bending and recovering

In order to further understand the bending, recovery, and stress

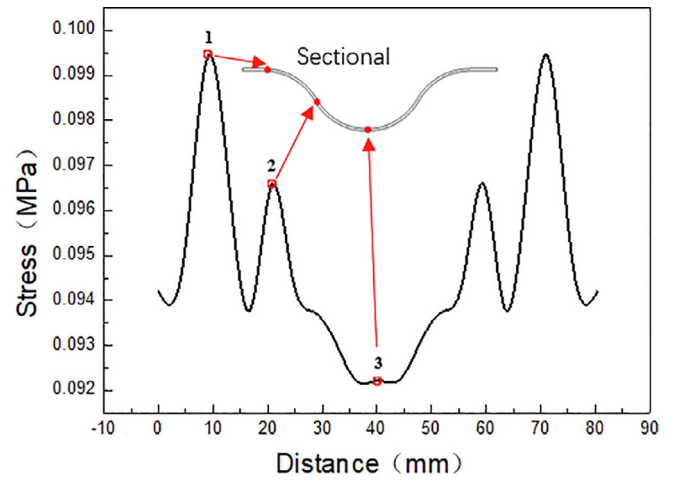


Fig. 22. Stress distribution along the transverse section.

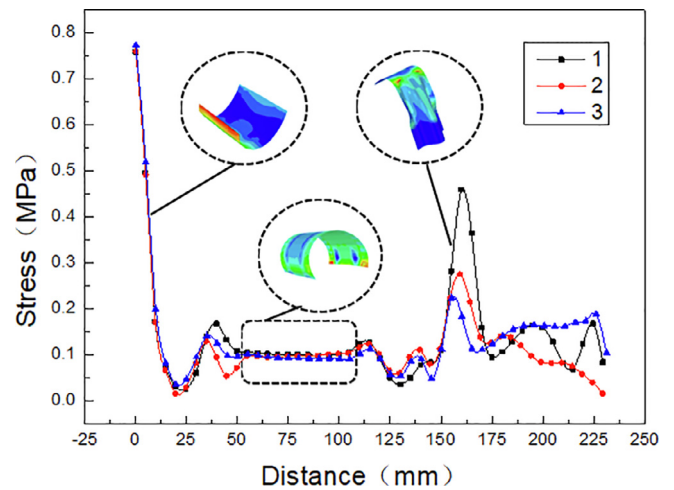


Fig. 23. Stress distribution along the longitudinal section.

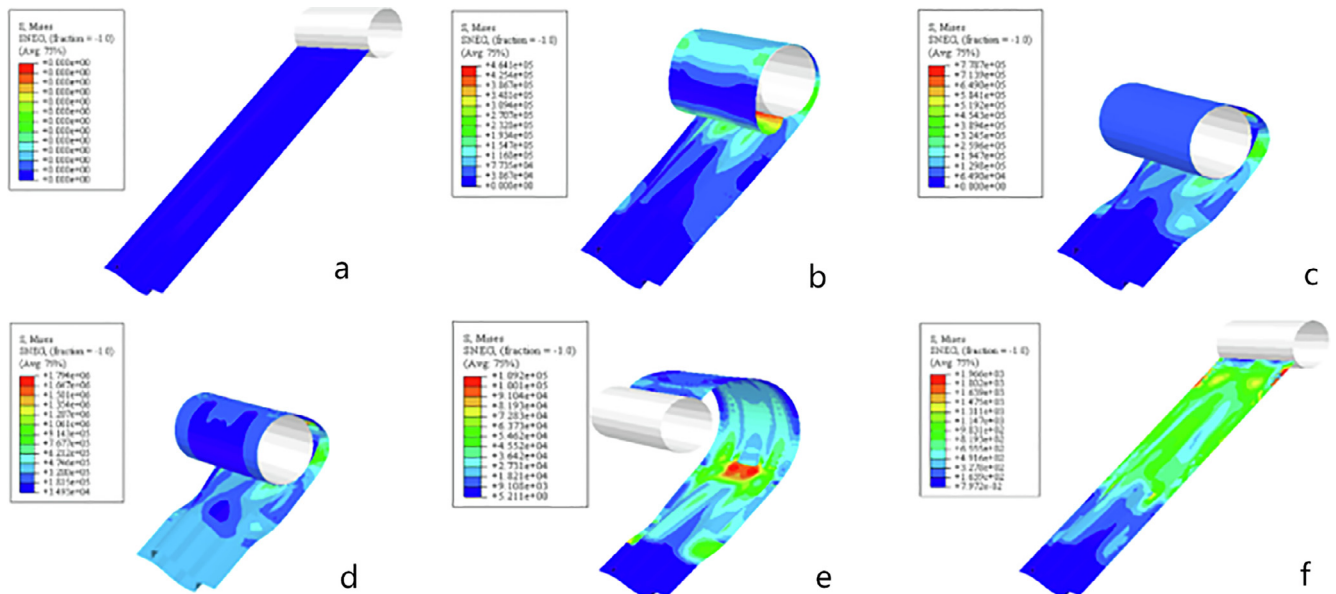


Fig. 21. Bending and recovery process of the LCCT: a) original shape; b) rising temperature and bend; c) keeping form; d) cooling; e) re-escalating temperature; f) recovering the original shape.

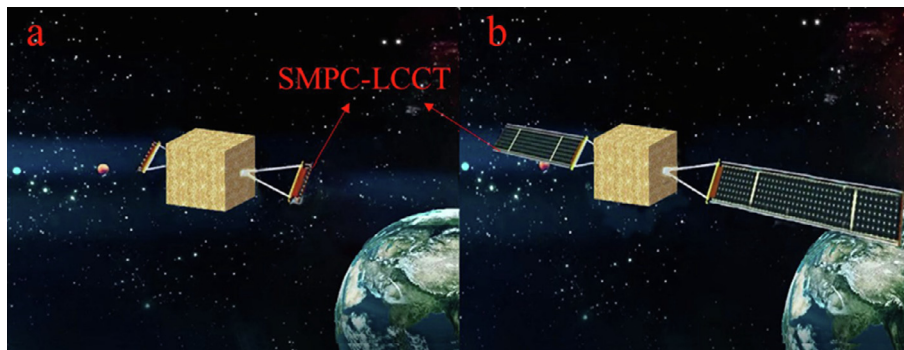


Fig. 24. Conceptual application in space deployable field: a) folding state of the flexible solar array; b) unfolding state of the flexible solar array.

distribution of the LCCT, a three-dimensional model of the LCCT was established in shell element with the software ABAQUS. The bending and recovery process of the LCCT was simulated as shown in Fig. 21. Compared with the LCCT recovery test (Fig. 19), it can be seen that the simulated bending process of shape of the LCCT is basically consistent with the actual bending shape, and the simulated recovery process is basically consistent with the experimental heating recovery process. The maximum stress value occurs in the bending process, which is 1.76 MPa and far less than the failure stress of shape memory polymer composites, therefore, it is reasonably inferred that LCCT will be safe in service.

The LCCT structure mainly carries out the load-bearing function in its rolled state. Therefore, this paper focuses on the bending morphology and stress changes along the transverse section and longitudinal section of the tube after bending. The three peaks in the stress curves of the transverse section are shown as 1, 2 and 3 respectively in Fig. 22, where the first point is situated at the transition point of the straight and circular transverse section of the LCCT, the second point is located at the transition area of the two arcs of the transverse section area, and the third point is situated at the apex of the middle arc of the transverse section area. It can be seen that the stress concentration is prone to occur in the transition area.

The following analysis also uses points 1, 2, and 3 to analyze the stress changes through the longitudinal section. In Fig. 23, the curved part is divided into three typical segments, the first segment is the end of the tube. Due to the rigid constraint between the end of the LCCT and the cylinder, the stress concentration occurred at the ends. As the bending radius increases, the stress decreases. The second segment is the middle part of the LCCT, which is bent along the circumference of the cylinder with the same bending radius; thus, the stress is approximately the same. The third section is the bending end of the LCCT. There is a peak value in the graph. This is because the bending end has a turning point from the bending state to the flat state, which is a sharp deformation, resulting in a stress concentration. Therefore, the stress variation analysis of the transverse section and the longitudinal section of the LCCT can help in understanding the whole bending process, and combined the analysis with the practical bending process, damage can be relatively reduced.

6. Potential applications of space deployable field

As a new type of deployable structure in space, the LCCT based on SMPC possesses outstanding merits of lightweight and foldability, stable deployment process. In addition, another obvious advantageous compared with conventional LCCT is that the thickness of the SMPC-based LCCT are adjustable, which can strengthen the stiffness of the composites and are more easily compacted into a small package. Based on this concept, Jinsong Leng's research group has developed a flexible solar array prototype based on SMPC LCCT structure, and will carry out space deployment verification test. As shown in Fig. 24, flexible LCCTs

are deployed on both sides of the solar array, which are then heated above the T_g . The connected flexible solar cell sheets are crimped and gathered, and after cooling, the solar array can maintain the gathering state in a small volume (shown in Fig. 24a). When the deployment mission is initiated, the LCCT are heated again to complete the self-deployment process (shown in Fig. 24b). Furthermore, the flexible LCCT structures can also be applied as a rotating hinge and used as a stretching arm for other deployment space structures. In summary, the SMPC-based LCCT has been and will continue to be of potential use in deployable space structures due to its unique structural and material characteristics.

7. Conclusion

Comparing with the traditional LCCT structure, the LCCT structure based on SMPC are actuated by electric heating, which demonstrated the advantages of stable deployment speed, controllable deployment process, lightweight, and high specific stiffness after cutting off electricity. Apparently, it has potential in space deployable field. Several conclusions can be summarized as follows:

- The basic mechanical properties of the material were obtained. The T_g of the epoxy resin is 150 °C determined by DMA test and the variable stiffness characteristics of the material were verified. After conducting the tensile and bending experimental results, +45°/-45° laminate was selected as the layering sequence. The variations of modulus, strength, elongation and the types of failure of the material with temperature were obtained.
- The strain distribution on the surface of lenticular shell was determined from a DIC test. The results show that the strain value on the transverse section has good symmetry along the middle longitudinal section, and the strain value on the longitudinal section has good similarity. The recovery test of the LCCT determined that 70 W is the optimum actuation power while obtaining the temperature distribution during the recovery process. Besides, the repeated bending recovery test showed that the LCCT have good repeatability within 30 deformation cycles.
- From the finite element simulation results during the bending process, stress concentration main occur at the turning point on the transverse section of the LCCT. The longitudinal section is divided into three typical segments. The stress distribution in the middle segment is uniform and low, while the deformation of the upper end segment and the lower end segment of the LCCT is complicated, and stress concentration may occur. In future study, it will focus on optimize the deformation of the ends of the LCCT and reduce the stress concentration during bending to achieve a wide application of this structure.

Acknowledgements

This work is supported by the National Natural Science Foundation of China (Grant No. 11632005, 11672086).

References

- [1] Leng J, Lan X, Liu Y, Du S. Shape-memory polymers and their composites: stimulus methods and applications. *Prog Mater Sci* 2011;56:1077–135.
- [2] Lendlein A, Kelch S, Kratz K, Schulte J. Shape-memory Polymers. *Angew Chem* 2002;41:2034–57.
- [3] Lendlein A, Schmidt AM, Langer R. AB-polymer networks based on oligo(epsilon-caprolactone) segments showing shape-memory properties. *PNAS* 2001;98:842–7.
- [4] Heuchel M, Sauter T, Kratz K, Lendlein A. Thermally induced shape-memory effects in polymers: Quantification and related modeling approaches. *J Polym Sci, Part B: Polym Phys* 2013;51:621–37.
- [5] Nguyen TD, Jerry Qi H, Castro F, Long KN. A thermoviscoelastic model for amorphous shape memory polymers: Incorporating structural and stress relaxation. *J Mech Phys Solids* 2008;56:2792–814.
- [6] Yang Q, Li G. Temperature and rate dependent thermomechanical modeling of shape memory polymers with physics based phase evolution law. *Int J Plast* 2016;80:168–86.
- [7] Abdin Y, Jain A, Verpoest I, Lomov SV. Mean-field based micro-mechanical modelling of short wavy fiber reinforced composites. *Compos A Appl Sci Manuf* 2016;91:472–83.
- [8] Lin JR, Chen L. Study on shape-memory behavior of polyether-based polyurethanes. I. Influence of the hard-segment content. *Applied Polymer. Science* 1998;69:1563–74.
- [9] Lin JR, Chen L. Study on shape-memory behavior of polyether-based polyurethanes. II. Influence of soft-segment molecular weight. *Applied Polymer. Science* 1998;69:1575–86.
- [10] Liu Y, Lv H, Lan X, Leng J, Du S. Review of electro-active shape-memory polymer composite. *Compos Sci Technol* 2009;69:2064–8.
- [11] Ohki T, Ni QQ, Ohsako N, Iwamoto M. Mechanical and shape memory behavior of composites with shape memory polymer. *Compos A Appl Sci Manuf* 2004;35:1065–73.
- [12] Lu H, Yu K, Sun S, Liu Y, Leng J. Mechanical and shape-memory behavior of shape-memory polymer composites with hybrid fillers. *Society of Chemical Industry*. 2010;59:766–71.
- [13] Mu T, Liu L, Lan X, Liu Y, Leng J. Shape memory polymers for composites. *Compos Sci Technol* 2018;160:169–98.
- [14] Mu T, Liu L, Lan X, Liu Y, Leng J. Shape memory polymer and its composite: function and application. *Comprehensive Composite Materials* 2018;II:454–86.
- [15] Lan X, Liu Y, Lv H, Wang X, Leng J, Du S. Fiber reinforced shape-memory polymer composite and its application in deployable hinge in space. *American Institute of Aeronautics and Astronautics* 2009.
- [16] Galletly DA, Guest SD. Bistable composite slit tubes. II. A shell model. *Int J Solids Struct* 2004;41:4503–16.
- [17] Hoang B, White S, Spence B, Kiefer S. Commercialization of Deployable Space Systems' roll-out solar array (ROSA) technology for Space Systems Loral (SSL) solar arrays. *Institute of Electrical and Electronics Eng* 2016.
- [18] Jafrancesco D, Sansoni P, Francini F, Contento G, et al. Mirrors array for a solar furnace: Optical analysis and simulation results. *Renew Energy* 2014;63:263–71.
- [19] Bai J, Xiong J, Gao J, Yi X. Analytical solutions for predicting in-plane strain and interlaminar shear stress of ultra-thin-walled lenticular collapsible composite tube in fold deformation. *Compos Struct* 2013;97:64–75.
- [20] Bai J, Xiong J, Gao J, Yi X, Zhang Z, He X, et al. Fabrication and validation of collapsible composite lenticular tubes. *Chin Soc Aeronautics Astronautics* 2011.
- [21] Hu Y, Chen W, Gao J, Hu J, Fang G, Peng F. A study of flattening process of deployable composite thin-walled lenticular tubes under compression and tension. *Compos Struct* 2017;168:164–77.
- [22] Block J, Straubel M, Wiedemann M. Ultralight deployable booms for solar sails and other large gossamer structures in space. *International Astronautical Congress* 2011.
- [23] Bai J, Xiong J. Temperature effect on buckling properties of ultra-thin-walled lenticular collapsible composite tube subjected to axial compression. *Chin J Aeronaut* 2014;27:1312–7.
- [24] Wu X, Zheng H, Liu Y, Leng J. Thermomechanical property of epoxy shape memory polymers. *Int J Mod Phys B* 2010.
- [25] Liu T, Liu L, Yu M, Li Q, Zeng C, Lan X, et al. Integrative hinge based on shape memory polymer composites: material, design, properties and application. *Compos Struct* 2018;206:164–76.
- [26] Ramakers-van Dorp E, Haenel T, Sturm F, Möglinger B, Hausnerova B. On merging DMA and microindentation to determine local mechanical properties of polymers. *Polym Test* 2018;68:359–64.
- [27] Lahelin M, Aaltio I, Heczko O, Söderberg O, Ge Y, Löfgren B, et al. DMA testing of Ni–Mn–Ga/polymer composites. *Compos A Appl Sci Manuf* 2009;40:125–9.
- [28] Vanlanduit S, Vanherzeele J, Longo R, Guillaume P. A digital image correlation method for fatigue test experiments. *Opt Lasers Eng* 2009;47:371–8.
- [29] Wang Changguo, Wang Yafei. The mechanical design of a hybrid intelligent hinge with shape memory polymer and spring sheet. *Compos B Eng* 2018;134:1–8. [10.1016/j.compositesb.2017.09.039](https://doi.org/10.1016/j.compositesb.2017.09.039) <https://linkinghub.elsevier.com/retrieve/pii/S1359836817303116>.